J. Materials, Conc. Struct., Pavements., JSCE, No.627/V-44, 289-303, 1999 August

NUMERICAL ANALYSES OF REINFORCED CONCRETE STRUCTURES USING SPRING NETWORK MODELS

Shigehiko SAITO[1] and Hiroshi HIKOSAKA[2]

[1]Student Member of JSCE, M. Eng., Graduate Student, Dept. of Civil Eng., Kyushu University
(Hakozaki 6-10-1, Higashi-ku, Fukuoka 812-8581, Japan)
[2]Member of JSCE, Dr. Eng., Professor, Dept. of Civil Eng., Kyushu University
(Hakozaki 6-10-1, Higashi-ku, Fukuoka 812-8581, Japan)

Computer modelings are one of the most suitable and promising approaches for comprehensively understanding the mechanisms of failure in concrete. This paper presents a practical, computationally efficient procedure for analyzing fracture of reinforced concrete structures. Concrete material is represented by a rigid-body-spring model with random geometry. Rather than averaging the effects of reinforcing over a regional material volume, reinforcing material is explicitly modeled using a beam- and linkage-spring. The spring network gives reasonable predictions of fracture behavior in reinforced concrete structures. Numerical predictions are compared with experimental results of reinforced concrete piers and beams.

Key Words: rigid-body-spring model, spring networks, random geometry, reinforced concrete structures, fracture, shear failure

1. INTRODUCTION

Reasonable and economical design for concrete structures requires the accurate comprehension of the deformation and stress interactions not only under service loadings, but also at the ultimate limit state. Both experimental and numerical investigation of materials and structures should be incorporated into the design process. Numerical methods for predicting the performance of reinforced concrete structures are becoming more effective with advances in computing technology. Since Ngo and Scordelis[1] applied finite element technique to a reinforced concrete structure in 1967, there have been many researches concerning the finite element idealization of concrete structures. One of the research interests for concrete structures is to investigate crack formation and propagation in concrete. Smeared cracking model has been typically used for presentation of concrete cracks, where the effects of cracks are assumed to be smeared out in a continuous fashion. Although such methods provide reasonable predictions for loading capacity, it is hard to obtain realistic crack patterns. Advanced design processes will, however, require direct understandings of damage condition and failure mode from numerical predictions.

Discrete methods have advantages to modeling of material discontinuity relative to continuum models like most finite element approaches. A rigid-body-spring model is one of those discrete approaches, which was first developed by Kawai[2]. Concrete is modeled as an assemblage of rigid particles interconnected along their boundaries through flexible interfaces. The interfaces may be viewed as springs, whose initial properties can be set to approximate the overall elastic properties of the continuum. The Kawai's spring model has been modified for analyzing damage evolution in brittle polycrystalline solids, where the material is randomly discretized by using Voronoi diagrams in order to reduce mesh bias on the fracture conditions[3]. The model has been also applied to analyzing fracture processes in cementitious composites at the meso-level[4]. The mesostructure components, such as the matrix, aggregate inclusion and matrix-inclusion interface, are explicitly modeled. Springs are assigned different properties to reflect the characteristic of each phase. The crack initiation and propagation in heterogeneous brittle materials have been well simulated in the analysis. Numerical applications to reinforced concrete structures have been given by averaging the effects of reinforcing over a regional material volume or modeling reinforcing material as a rigid element[5]. In such analyses, the reinforcing ar-

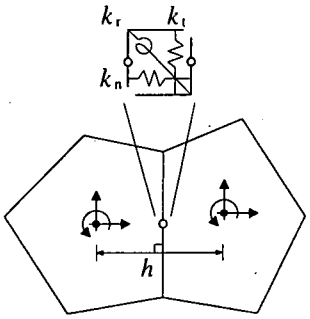

Fig. 1 Two-particle assembly

rangement will restrict the concrete mesh discretizations, so that there is difficulty in introducing the random geometry using Voronoi diagrams.

This paper presents the discrete models of concrete material and steel reinforcement, which can lead to reasonably accurate prediction of structural behavior of reinforced concrete, especially on crack patterns. The model for concrete material is initiated from the Kawai's spring model. The simplicity of the concrete model provides a natural means for incorporating discrete models of continuous reinforcement. Rather than averaging the effects of reinforcing over a regional material volume, each reinforcement is explicitly modeled using a series of regular beam elements. The bond-slip characteristics between reinforcing steel and concrete material are represented by special linkage elements that are placed periodically along the reinforcement-concrete interface. Furthermore, reinforcing material can be placed anywhere in the specimen irrespective of the matrix mesh geometry. The analysis of complicated reinforcing arrangements, including the addition of main reinforcing bars, is greatly facilitated. The spring network is attractive due to their simplicity, freedom in mesh generation, and providing a discrete representation of fracture. Potential of the approach is demonstrated through analyses of T-shape bridge piers under eccentric loading and reinforced concrete beams without shear reinforcement.

2. CONCRETE MATERIAL MODEL

The Kawai's rigid-body-spring model can be considered as one of spring network models that consist of regularly or randomly distributed nodal sites interconnected by springs. Such networks are composed of central force springs or beam-springs as discretizations of a continuum material[6),7)]. The rigid-body-spring model is a special type of beam-spring network and the beam-spring networks generally perform better than other standard networks for fracture simulation in homogeneous isotropic materials. The similarities between the rigid-body-spring and ordinary beam-spring approaches are discussed in Bolander and Saito[8)]. The spring network approach is also similar to microplane models[9)] in that material response is defined local to planes (or line segments for two-dimensional analysis) with arbitrary inclination in the material.

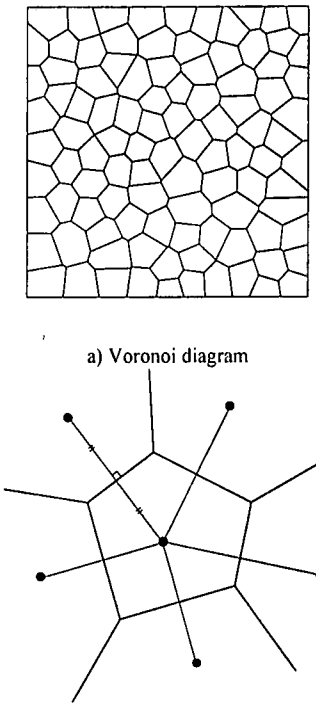

a) Voronoi diagram

b) Voronoi cell

Fig. 2 Random geometry with Voronoi diagram

The rigid-body-spring network represents a continuum material as an assemblage of rigid particle elements interconnected by springs. The response of the spring network model provides comprehension of the interaction between particles instead of the internal behavior of each particle based on a continuum mechanics. The model is therefore suited towards problems where material discontinuities are dominant. The fracture in composite materials like concrete may be modeled as discretizations of a continuum using the spring network, since such brittle materials behave as a discontinuum when fracture occurs and progresses.

(1) Spring network with random geometry

Concrete is modeled as an assemblage of rigid particles interconnected along their boundaries by springs (**Fig. 1**). Each rigid particle has two translatory and one rotational degrees of freedom defined

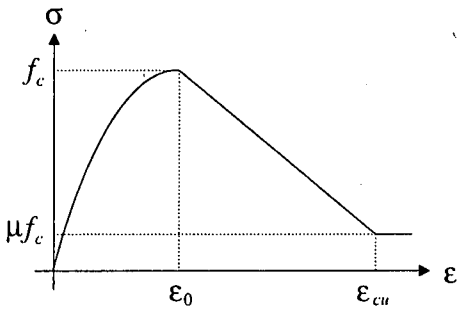

Fig. 3 Compression model

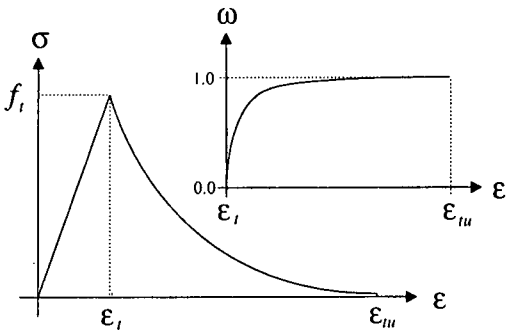

Fig. 4 Tension softening model

at some point within its interior. The interface between two particles consists of three individual springs. Normal, tangential, and rotational springs act at the facet midpoint, whose initial properties can be set to approximate the elastic properties of the continuum. The system equilibrium equations are constructed from the stiffness and load contributions of each two-contiguous-particle assembly in the conventional manner[2].

Since concrete cracks initiate and propagate along interparticle boundaries, mesh design may constrain the fracture directions. That is, the crack pattern is strongly affected by the local structure of the network. As the model simplicity provides considerable freedom in mesh layout, a random geometry is introduced using a Voronoi diagram for minimizing mesh bias on crack direction[3),10]. The Voronoi diagram is the collection of Voronoi cells as shown in **Fig. 2a**. That is, each Voronoi cell is a concrete rigid particle. The Voronoi cell is constructed by a set of perpendicular bisectors of nuclei that are closer to the nucleus of the cell than all other nuclei (**Fig. 2b**). Since those nuclei are randomly generated, a random geometry of a rigid-body-spring network can be obtained. The mesh generation of rigid particles is highly automated. A more detailed description of Voromoi diagrams is given in Preparata and Shamos[11], for example.

The recommendation of the size of Voronoi cells has not been given. The use of larger cell size will restrain possible crack development and propagation direction. In the case that the cell size is too small, the spring properties, however, require the different material modelings such as a three-phase modeling: matrix, aggregate, and matrix-aggregate interface. Therefore the size of Voronoi cells will be at least larger than the maximum aggregate size. The finer discretizations are preferable in order not to restrict potential crack directions and to obtain the realistic crack patterns.

The rigid-body-spring network provides a discrete rather than a continuum representation of fracture. One of the fundamental issues on such discrete methods is the potential in representing an elastic continuum. Bolander and Saito[8] indicates the significance of the network design in a rigid-body-spring network with random geometry. A random geometry lattice of ordinary beam-spring is generally not homogeneous under uniform strain[7]. A rigid-body-spring network with random geometry is not elastically uniform when the computational degrees of freedom are set on the cell centroids as usual. Rather than the centroids, the nuclei of the Voronoi cells should be used as the computational degrees of freedom so that the rigid-body-spring network with random geometry is elastically uniform. In order to maximize the degree of isotropy with respect to possible crack direction, the distribution of nuclei defining the Voronoi diagrams is important. The network's ability to model a uniform strain field allows the reasonable representation of a continuum material in the discrete approaches.

(2) Material model

In a rigid-body-spring network the fracture criterion is not based on a tensorial measure of stresses, but utilizes the average stresses acting normal and tangential to the particle interface. The criterion is therefore rather simply constructed. That is, uniaxial stress-strain relationships can be introduced into the individual spring.

The local stiffnesses k_n, k_t, and k_r are set to approximate the elastic properties at the continuum level[2]. Normal springs are set to represent tensile and compressive properties of concrete. The material under compression shows the nonlinear behavior up to the compressive strength and after the peak the softening branch exists until failure (**Fig. 3**). The hardening behavior up to the compressive strength is modeled by using a parabolic curve[12]. The stress-strain relationships in compression are idealized as the following equations.

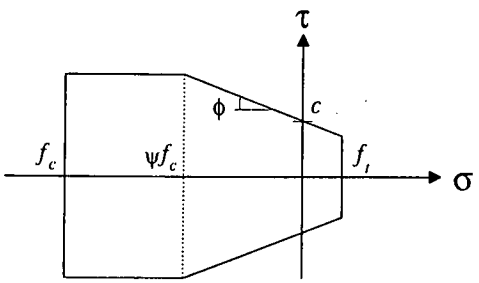

Fig. 5 Mohr-Coulomb criterion for shear spring

$$\sigma = \begin{cases} E\varepsilon - \dfrac{E}{2\varepsilon_0}\varepsilon^2 & (\varepsilon \le \varepsilon_0) \\ f_c - \dfrac{(f_c - \mu f_c)}{(\varepsilon_{cu} - \varepsilon_0)}(\varepsilon - \varepsilon_0) & (\varepsilon_0 < \varepsilon \le \varepsilon_{cu}) \\ \mu f_c & (\varepsilon > \varepsilon_{cu}) \end{cases} \quad (1)$$

where E is the modulus of elasticity, f_c is the compressive strength, and $\varepsilon_0 = 2f_c/E$. The ultimate strain ε_{cu} is set to $4\varepsilon_0$, and μ is set to 0.2 in this study.

Concrete under tension behaves linearly elastic up to the tensile strength, then the stress-strain relationship exhibits strain softening until failure (**Fig. 4**). The fracture energy can be introduced in order to define the softening branch and avoid the mesh size dependence. A number of articles have proposed the tension softening curves, such as linear, functional, and polynomial curves[13]. This study uses the simple exponential approximation[14]. Introducing the damage parameter ω, the tension softening curve is defined by

$$\sigma = (1-\omega)E\varepsilon \quad (2)$$

where

$$\begin{cases} \omega = 0 & (\varepsilon \le \varepsilon_t) \\ \omega = 1 - \dfrac{\varepsilon_t}{\varepsilon}\exp\left[-\dfrac{\kappa}{\varepsilon_{tu}}(\varepsilon - \varepsilon_t)\right] & (\varepsilon > \varepsilon_t) \end{cases} \quad (3)$$

in which $\varepsilon_t = f_t/E$; f_t is the tensile strength. The damage parameter ω represents the degree of damage and varies from $\omega = 0$ (no damage) up to $\omega = 1$ (complete damage). The constant parameter κ adjusts the degree of exponential softening; $\kappa = 5$ provides an approximation to the strain softening witnessed in direct tension testing. The ultimate strain ε_{tu}, where the stress is assumed to be zero, is approximately calculated by the following equation.

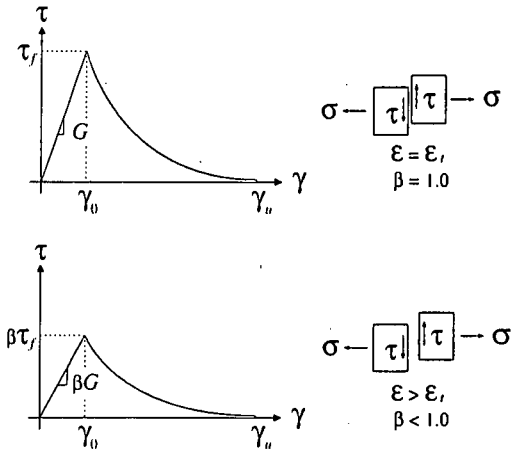

Fig. 6 Shear softening model for cracked interfaces

$$\varepsilon_{tu} \approx \kappa\left(\frac{G_f}{f_t h} - \frac{f_t}{2E}\right) \quad (4)$$

where G_f is the fracture energy which represents the amount of energy consumed to create a crack of one unit area. h indicates the characteristic length which is the sum of the perpendicular lines from adjacent computational points to the boundary segment as shown in **Fig. 1**. The change of ε_{tu} according to the mesh size (that is, the length h) reduces the mesh dependence in the analysis.

When the normal spring reaches the strength f_t or f_c, the force in the rotational spring is released and the local stiffness k_r is set to zero.

Tangential springs represent the shear transferring mechanism of concrete. The shear strength is assumed to follow the Mohr-Coulomb type criterion with the tension and compression caps[5),15)] as shown in **Fig. 5**. c and ϕ are the cohesion and internal friction angle, respectively. ψ is the constant parameter and set to 0.5. The shear fracture criterion is therefore expressed as

$$\frac{\tau^2}{\tau_f^{\,2}} \ge 1 \quad (5)$$

where

$$\tau_f = \begin{cases} c - \sigma\tan\phi & (\sigma \ge \psi f_c) \\ c - \psi f_c\tan\phi & (\sigma < \psi f_c) \end{cases} \quad (6)$$

After the shear stress reaches the yield strength, the stress moves on the yield surface until the shear strain reaches the ultimate strain γ_u. The force in the shear spring is released and the local stiffness k_t is

set to zero when the shear strain exceeds the ultimate strain. The ultimate strain is set to 4000μ in this study.

For cracked interfaces, a softening branch is assumed after shear stress reaches the yield strength. The same softening rate as that of the tension softening model is assumed to represent the stress-strain relationship in shear. That is,

$$\tau = (1-\lambda)G\gamma \tag{7}$$

where

$$\begin{cases} \lambda = 0 & (\gamma \le \gamma_0) \\ \lambda = 1 - \dfrac{\gamma_0}{\gamma}\exp\left[-\dfrac{\kappa}{\gamma_u}(\gamma-\gamma_0)\right] & (\gamma > \gamma_0) \end{cases} \tag{8}$$

in which G is the shear stiffness; $\gamma_0 = \tau_f/G$. The parameter λ represents the degree of damage as with the parameter ω of the tension softening model. The ultimate strain γ_u will be defined by the shear (mode II) fracture energy. The mode II fracture energy is hardly available, although many researchers have attempted to measure a pure mode II fracture energy[16]. The ultimate strain of cracked interfaces is therefore assumed to be the same as that of uncracked interfaces (that is, $\gamma_u = 4000\mu$) in this study.

The shear transferring capacity at the cracked interface changes according to crack opening. In order to take account of this effect, the shear stiffness is reduced by using a function of the strain normal to the crack. By introducing the reduction factor β, the shear stress-strain relationship for the cracked interface is finally expressed as

$$\tau = (1-\lambda)G_{cr}\gamma \tag{10}$$

where

$$G_{cr} = \beta G \tag{11}$$

The reduction factor β is set to $1-\omega$, which varies from 1 (no damage) down to 0 (complete damage), but the constant parameter κ is adjusted to 0.3 in order to provide an approximation to the shear stiffness reduction proposed by Aoyagi and Yamada[17]. Consequently, the stress-strain relationship of the tangential spring at the cracked interface is affected by two parameters; β degrades the shear stiffness according to crack opening and λ provides the softening branch after the shear stress reaches the strength, as shown in **Fig. 6**. Although the tangential springs are influenced by the condition of the normal springs, the effect of the tangential springs on the normal springs is not taken into consideration in this study. Furthermore, the shear model assumed here is not objective with respect to changes in mesh size. The model should be extended so that proper mode II fracture energy is consumed under shear deformation.

In the stress-strain relationship of both the normal and tangential springs, the unloading and reloading occur along the secant modulus.

3. REINFORCEMENT MODEL

Ueda *et al* [5] applied the Kawai's spring network model to analyzing reinforced concrete structures, where the effects of conventional steel reinforcing bars were smeared within the concrete particles. Thus, the perfect bond between the concrete and the reinforcing steel was assumed. Such model is generally practicable for concrete structures with complicated reinforcement, since the discrete modeling of reinforcement has difficulty in the mesh design.

The authors have developed an effective means for introducing continuous reinforcement into rigid-body-spring networks with random geometry[18]. Each continuous reinforcement (that is, steel bar) is explicitly modeled and can be positioned irrespective of the concrete particles. The bonding properties between the concrete and the reinforcing steel are introduced by special linkage elements.

(1) Discrete modeling of reinforcement

Reinforcement is represented by a series of regular beam elements. The beam nodes are attached to the concrete particles through zero-length link elements (**Fig. 7**). Assuming small rotations, the displacements (u_{1c}, v_{1c}) at the point of the linkage element (x_1, y_1) located on the particle will displace by the computational point (x, y). That is,

$$\begin{aligned} u_{1c} &= u - (y_1 - y)\theta \\ v_{1c} &= v + (x_1 - x)\theta \end{aligned} \tag{12}$$

where u, v, and θ are the two translatory displacements and one rotation of the particle computational point. Thus, the relative displacements between the concrete particle and the reinforcement end are expressed by

$$\mathbf{d} = \mathbf{B}\mathbf{u} \tag{13}$$

in which

$$\mathbf{B} = \begin{bmatrix} -1 & 0 & (y_1 - y) & 1 & 0 & 0 \\ 0 & -1 & -(x_1 - x) & 0 & 1 & 0 \\ 0 & 0 & -1 & 0 & 0 & 1 \end{bmatrix} \tag{14}$$

where $\mathbf{u}^T = [u, v, \theta, u_1, v_1, \theta_1]$; u_1, v_1, and θ_1 are the two translatory displacements and one rotation of

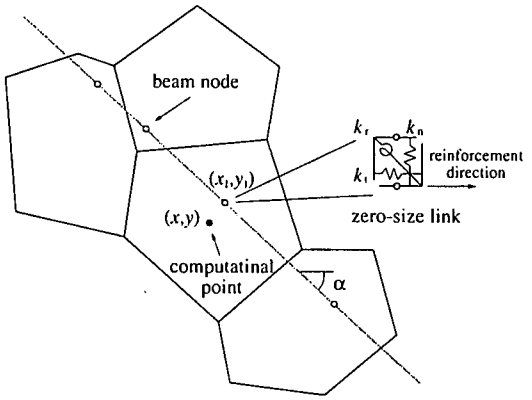

Fig. 7 Introducing reinforcement into a spring network

the beam end. $\mathbf{d}^T = [\delta_t, \delta_n, \phi]$; δ_t, δ_n, and ϕ are components of relative displacements in the tangential, normal, and rotational sense, respectively.

To obtain the local displacement components $\mathbf{d}^*$, it is necessary to use an appropriate strain transformation matrix **T**. That is

$$\mathbf{d}^* = \mathbf{T}\mathbf{d} \tag{15}$$

With α defined in **Fig. 7**, **T** is given by

$$\mathbf{T} = \begin{bmatrix} \cos\alpha & \sin\alpha & 0 \\ -\sin\alpha & \cos\alpha & 0 \\ 0 & 0 & 1 \end{bmatrix} \tag{16}$$

The element local stiffness matrix for the linkage element can be written by the following

$$\mathbf{k}_e = \mathbf{B}^T\mathbf{T}^T\mathbf{D}\mathbf{T}\mathbf{B} \tag{17}$$

where the material elasticity matrix is expressed as

$$\mathbf{D} = \begin{bmatrix} k_{L,t} & 0 & 0 \\ 0 & k_{L,n} & 0 \\ 0 & 0 & k_{L,r} \end{bmatrix} \tag{18}$$

$k_{L,t}$, $k_{L,n}$, and $k_{L,r}$ are the tangential, normal, and rotational spring stiffnesses of the linkage element, respectively.

Continuous reinforcement consists of a series of regular beam elements. Each beam element of reinforcement has axial, shear and flexural degrees of freedom at the nodes. The global displacement components at the beam node will be transformed to the local components by the same type of transformation matrix as for the linkage element.

Introduction of a continuous reinforcement is carried out by the use of a computer mouse or other preprocessing tools. Reinforcing steel can be positioned without regard to the concrete mesh design.

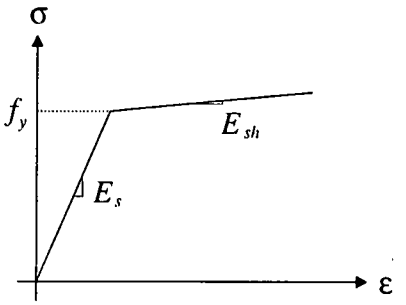

Fig. 8 Stress-strain relation for reinforcing steel

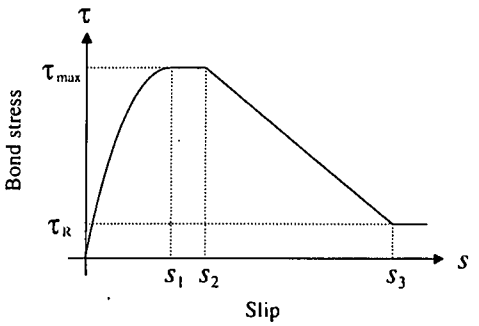

Fig.9 Idealization of bond stress-slip relationship

(2) Material model

Material stress-strain relation for steel reinforcing bars is idealized as a bilinear elastic strain-hardening plastic as shown in **Fig. 8**. The modulus of elasticity at the hardening branch E_{sh} is set to $0.01E_s$.

The bond-slip interaction between the concrete and the reinforcing steel strongly affects the crack condition and the stress in the reinforcement. The stress transfer will be represented by introducing the bond-slip relation into link elements. The spring parallel to the reinforcing bar is used to represent the bonding characteristics. The bond stress-slip relationships for conventional steel reinforcing bars are idealized as shown in **Fig. 9**, according to recommendations proposed by CEB-FIP[19]. The parameters in **Fig. 9** depend on the influencing factors: confinement, bond condition and concrete strength. The analysis here uses the values for confined concrete and assumes that the bond condition is good.

Stiffness normal to the reinforcing bar direction, and in the rotational sense, is set to the large value since the relative displacement is not expected.

In both the reinforcement and bond-slip model the unloading and reloading follows the initial stiffness.

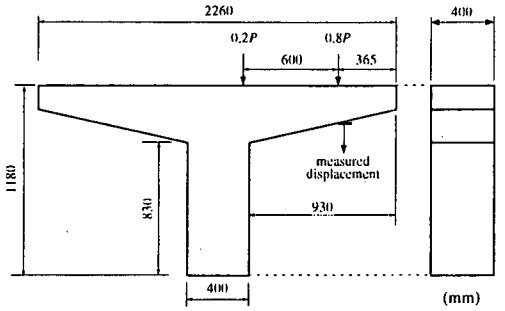

Fig. 10 Specimen dimensions and boundary conditions

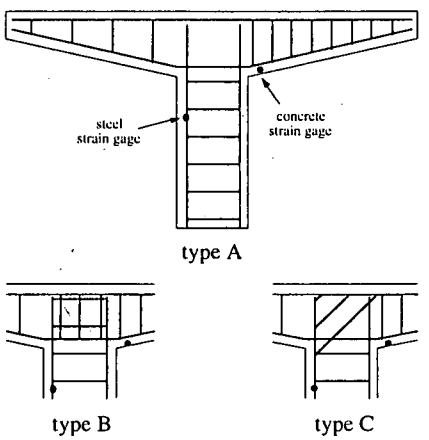

Fig. 11 Reinforcing arrangement

4. ANALYSIS APPLICATIONS

(1) T-shape piers under eccentric loading

A series of model tests was conducted to investigate the performance of reinforced concrete T-shape piers under eccentric loading[20]. The common geometry and boundary conditions through all the specimens are shown in **Fig. 10**. The stress state in the beam-to-column joint region of the T-shape piers under eccentric loading is similar to one in a knee joint subjected to bending moment (closing moment). In the knee joint which connects the beam and column, diagonal cracks occur due to closing moment, so that the appropriate reinforcing arrangement in the joint region is required in order to control those diagonal cracks[21]. Three types of the tested specimens differed in the reinforcing arrangement in the beam-to-column joint region (**Fig. 11**). The joint region of the type A is not reinforced, while the type B and C have additional reinforcing steel in their joint regions. **Fig. 12** shows the numerical models of T-shape piers fixed at the base; the specimen is discretized into 1500 rigid particles.

Table 1 Material properties

concrete	
Young's modulus	22 GPa
Poisson ratio	0.17
compressive strength	23 MPa
tensile strength	1.6 MPa
steel	
Young's modulus	210 GPa
yield strength	350 MPa

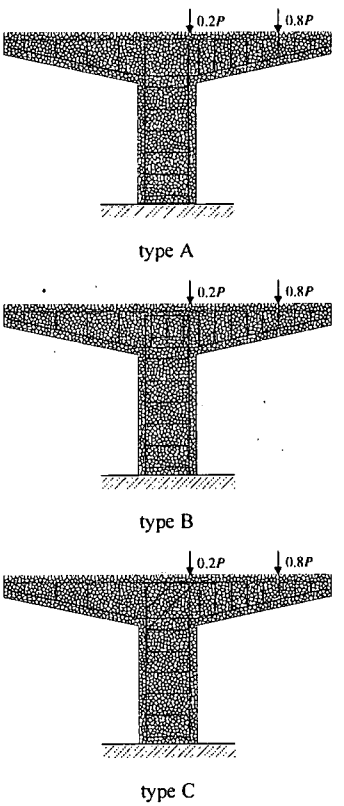

Fig. 12 Numerical models of reinforced concrete piers

Since the same spring network representation of the concrete material can be utilized through all the specimens, mesh construction is carried out with minimal effort. The material properties of concrete and steel are given in **Table 1**. The fracture energy G_f used to define tension softening curves is assumed to be 100N/m.

Comparisons of numerical predictions and experimental results for load-displacement (P-Δ) relations are shown in **Fig. 13**. The vertical displacement Δ was measured at the point indicated in **Fig. 10**. The

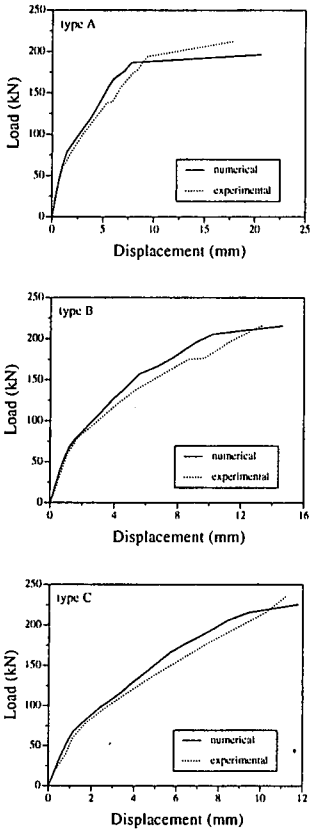

Fig. 13 Load-displacement curves

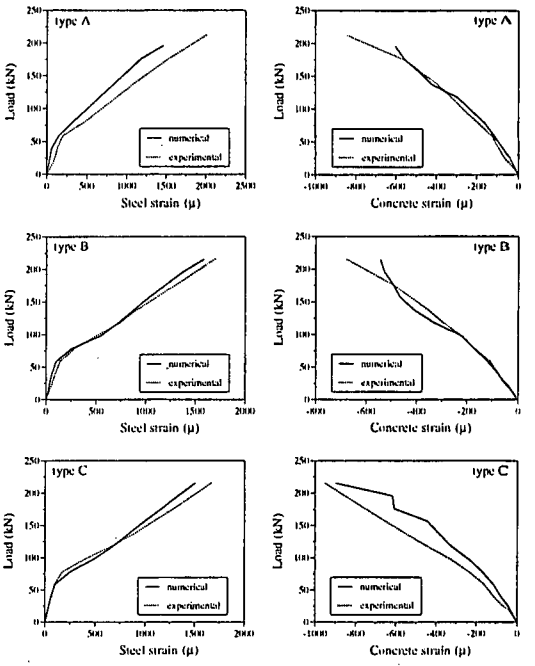

Fig. 14 Load-strain relations of steel and concrete

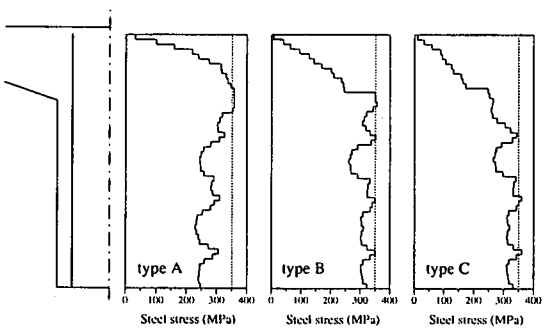

Fig. 15 Steel stress distributions in columns

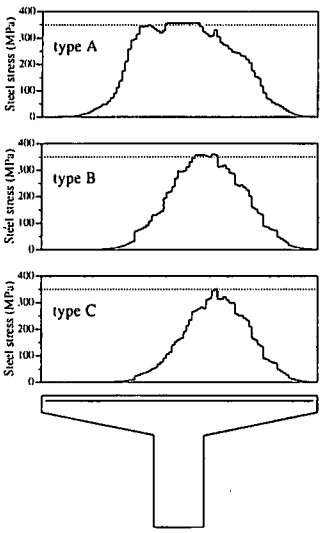

Fig. 16 Steel stress distributions in beams

monotonic envelopes are taken for comparison although the repeated incremental loading was used in the tests. The test did not examine the post-peak response. The type A failed by the large diagonal cracks in the beam-to-column connection region and the flexural cracks at the top of the column. The failure of the type B is composed of the diagonal cracks in the joint region and the flexural cracks in the column. The diagonal cracks also appeared in the joint region, yet the type C failed by the flexural cracks in the column. The numerical predictions on load-displacement responses reasonably agree with experimental results.

Comparisons for tensile strain of steel and compressive strain of concrete are shown in **Fig. 14**. The gage locations are indicated in **Fig. 11**. The numerical predictions show the same trends as the observations in the tests. It can be seen that the discrete representation of material using a rigid-body-spring network is valid for evaluating the nonlinear behavior of concrete.

Fig. 15 and **Fig. 16** show the stress distributions of

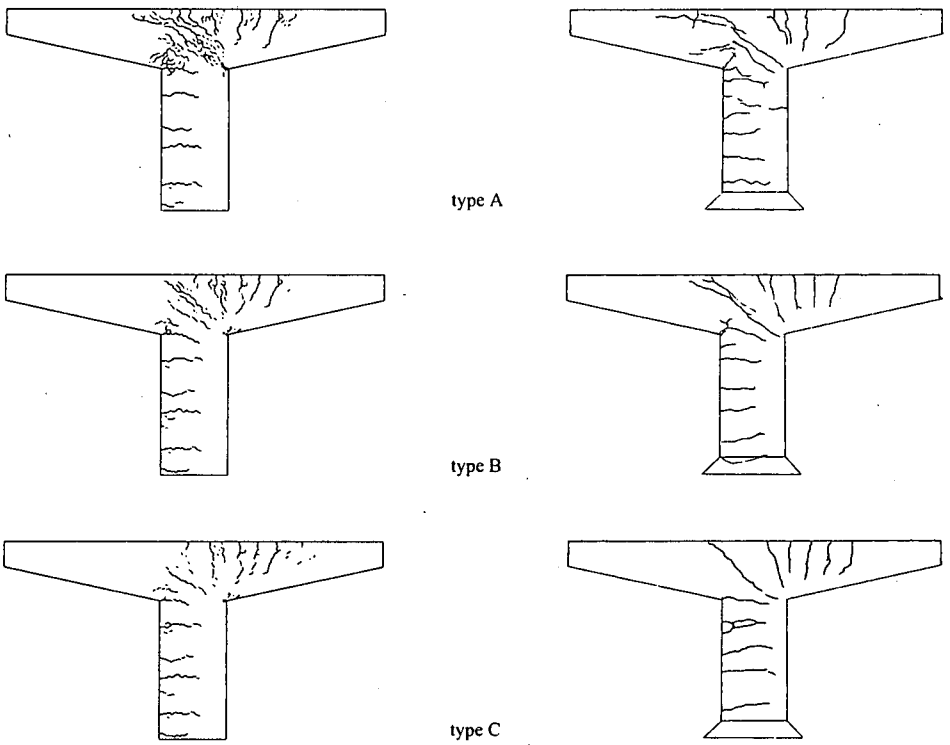

Fig. 17 Numerical crack patterns comparing with experimental observations

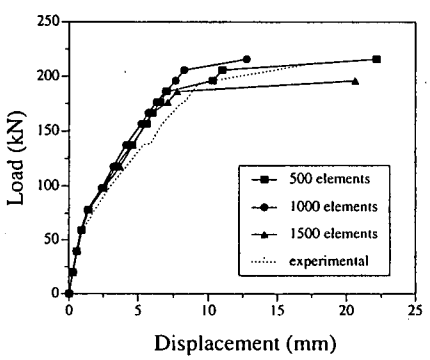

Fig. 18 Load-displacement relations for different mesh

reinforcing steel in the beam and column at the peak load. The broken lines in the figures indicate the yield strength of reinforcing steel. The joint region of the type A has less reinforcement, so that the stress concentrates in the joint region. Since the stress in the joint region of the type C is greatly reduced, the additional reinforcements are effective to control the fracture conditions in joint region. The stress distribution of the type B shows the middle condition between the type A and C.

Fig. 17 compares the crack patterns obtained from the numerical predictions with those from the experiments at the peak load. The type A and B specimens show large diagonal cracks in the beam-to-column joint region. The growth of diagonal cracks in the joint region of the type C is restrained by the additional diagonal reinforcements. The numerical crack patterns are close to the experimental observations in terms of number of cracks, crack locations, and angles of diagonal cracks in the joint region.

In general, fracture conditions and loading capacities of discrete models are highly influenced by mesh discretization. In order to investigate the mesh dependence on the number of elements, three different meshes are used for analyzing the type A. The number of elements is differed as 500, 1000, and 1500 elements; the average element size is 48, 34, and 28 mm, respectively. All the specimens are randomly discretized with Voronoi diagrams. The load-displacement responses are shown in **Fig. 18**. Although the analysis results exhibit some scatter for the loading capacity, the predictions are close to the experimental results. The mesh sensitivity has been greatly reduced by the use of random geometry and the softening models according to fracture energy.

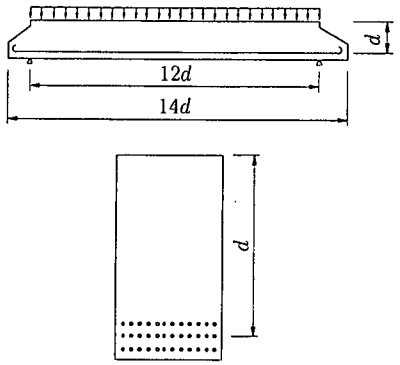

Fig. 19 Specimen dimensions and boundary conditions

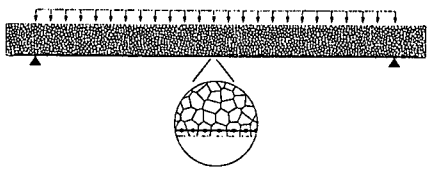

Fig. 20 Numerical model of specimen No. 7

(2) Reinforced concrete beams without shear reinforcement

The rigid-body-spring network model is applied to analyzing a series of simply supported reinforced concrete beams under uniform loading tested by Iguro *et al*[22]. Some numerical studies associated with their tests have been presented in a summary of round robin analyses designed by Japan Concrete Institute[23]. There was difficulty in analyzing the shear failure of the reinforced concrete beams. In a recent study presented by An *et al*[24], their finite element approaches have successfully predicted the shear failure mode of the beams.

Fig. 19 shows the specimen geometry and boundary conditions. The specimens did not include shear reinforcements, in order to investigate the size effect on shear strength. The ratio of loading span to effective depth was set to 12, in anticipation of shear failure mode. The test program differed in the effective depth of beams: 0.1, 0.2, 0.6, 1.0, 2.0, and 3.0 m. Specimen dimensions and material properties are shown in **Table 2** and **Table 3**, respectively.

Fig. 20 shows the mesh geometry of the largest beam. Each specimen is discretized into 1500 elements. The properties of steel reinforcing in numerical models are condensed into one level at the effective depth in order to reduce computational expense, although the test specimens have three levels of reinforcement. Note that all levels of reinforcing can be readily introduced in numerical models[8]. The number of reinforcing levels and concrete cover

Table 2 Specimen dimensions

No.	d (m)	loading span(m)	length (m)	height (m)	width (m)
1	0.1	1.2	1.4	0.12	0.16
2	0.2	2.4	2.8	0.22	0.16
3	0.6	7.2	8.4	0.66	0.3
5	1.0	12	14	1.2	0.5
6	2.0	24	28	2.1	1.0
7	3.0	36	42	3.1	1.5

Table 3 Material properties

No.	concrete				steel	
	E_c(GPa)	f_c(MPa)	f_t(MPa)	G_f(N/m)	E_s(GPa)	f_y(MPa)
1	23.3	20.6	1.85	70	210	440
2	22.9	19.7	1.87	70	210	440
3	23.5	21.1	1.81	70	210	440
5	23.8	21.9	2.23	70	210	370
6	26.0	28.5	2.73	100	210	370
7	24.6	24.3	2.19	100	210	360

thickness influences the number of cracks, crack spacing, and width, so that the further research will be required in this aspect.

Numerical predictions of load pressure-midspan displacement responses are compared with the experimental results as shown in **Fig. 21**. Specimen gravity loads are negligible for No. 1 and No. 2. For No.6 and No.7, the gravity loads can be excluded due to their loading condition[22]. The analyses take account of the gravity loads for only No.3 and No.5. The trends in the numerical predictions agree well with the experimental results. In both the analyses and tests, the specimens No. 1 and No. 2 failed with flexural modes; diagonal tension failure occurred for the rest of specimens.

Load pressure-steel reinforcing bar strain relations at the midspan are shown in **Fig. 22**. Numerical analyses provide sufficient predictions of the steel strain although the multi-level arrangement of steel reinforcing is simply modeled.

Fig. 23 shows the numerical predictions of crack pattern at the failure load comparing with the observations in the tests. The numerical model predicts not only distributed flexural cracks but also diagonal tension cracks successfully. **Fig. 24** shows the history of crack growth for the specimen No. 3; the sampling points A, B, and C are indicated in **Fig. 21**. In

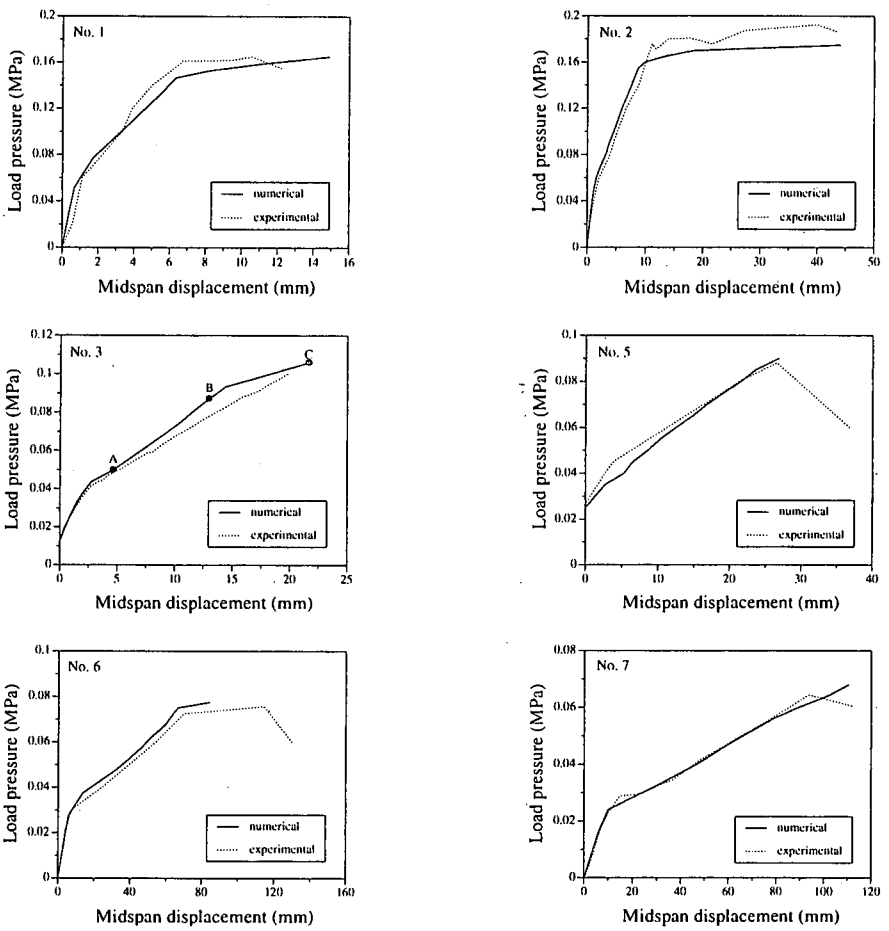

Fig. 21 Load pressure-midspan displacement curves

the early stage of loading, flexural cracks occur and distribute near midspan, then develop towards both sides of the beam. As the loads increase diagonal cracks appear nearby the supports and propagate together with flexural cracks. The rigid-body-spring network model with random geometry can provide the realistic crack patterns relative to predictions given by finite element approaches with smeared crack model. The failure modes can be confirmed by both the load-displacement curve and the deformed geometry (crack pattern).

Fig. 25 shows the nominal shear strength computed from the peak load. The analysis results agree well with the experimental results with the exception of No.1 and No.2. The numerical model predicts the size effect on shear strength successfully.

Analyses without shear softening are carried out in order to confirm the validity of the proposed shear softening model. Only the parameter λ is excluded from the proposed shear model, so that all the other conditions are kept the same as the previous analysis. The specimens No.3, 5, 6, and 7, which are failed in shear mode are analyzed. The load pressure-displacement responses without shear softening are shown in **Fig. 26**. All the results without shear softening show the higher loading capacity. The specimens No.3 and No.5 failed with shear mode, while the specimens No.6 and No.7 showed bending failure mode. The shear softening model greatly affects on the loading capacity and failure mode. The same tendency is observed in the finite element analysis[24], yet the stiffness behavior of the reinforced concrete member is also influenced by the shear softening in the proposed discrete approach. The discrete model will be sensitive to the shear modeling in the tangential springs. Further investigation should be needed so that proper shear transferring behavior is introduced.

In order to investigate the model sensitivity to the number of elements (that is, element size) three different meshes are used for analyzing the specimen No. 7. The number of elements is differed as 500, 1000, and 1500 elements. The average element size is 570, 400, and 330 mm, respectively. The load-

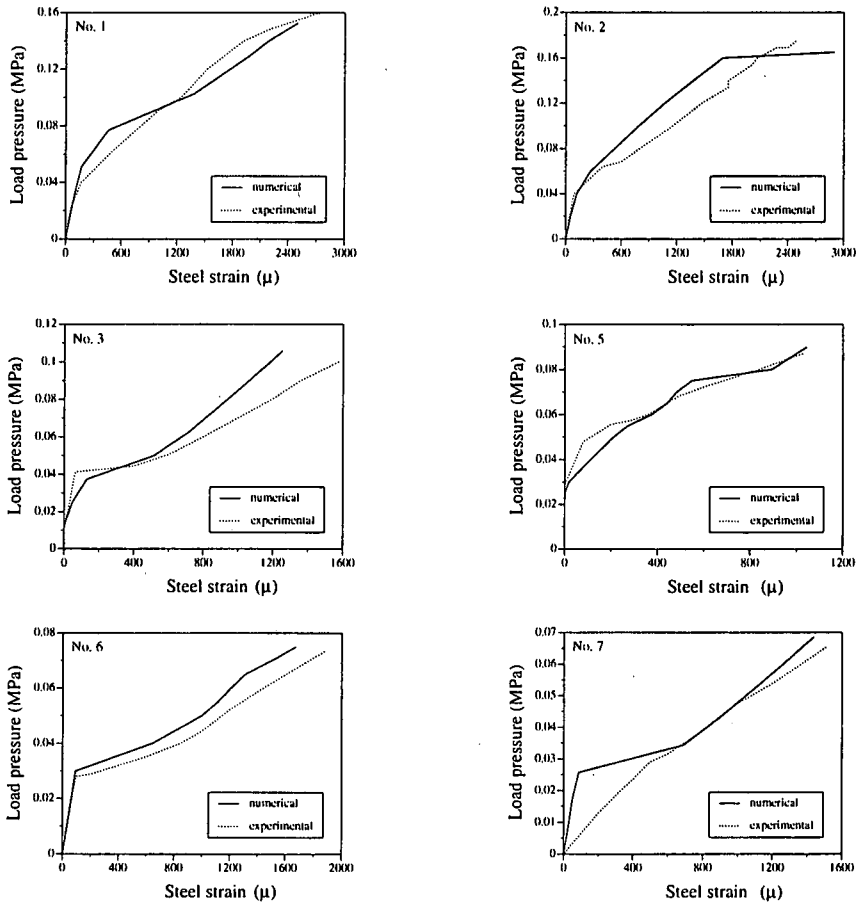

Fig. 22 Load pressure-steel strain curves

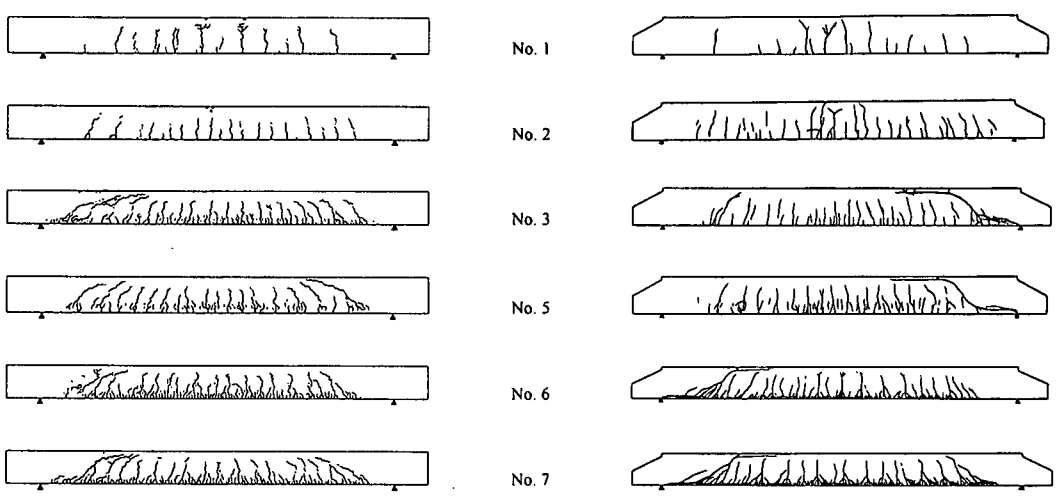

a) numerical results

b) experimental results[13]

Fig. 23 Crack patterns

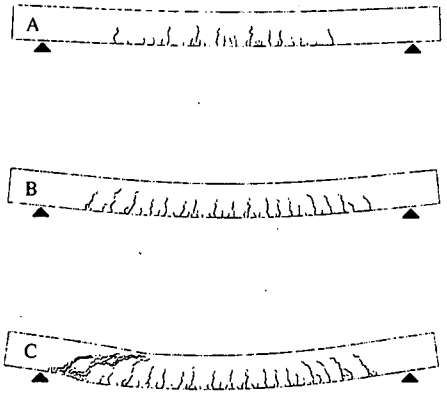

Fig. 24 Historical crack patterns of specimen No. 3

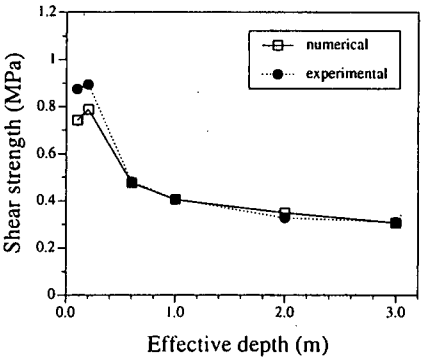

Fig. 25 Size effect on shear strength

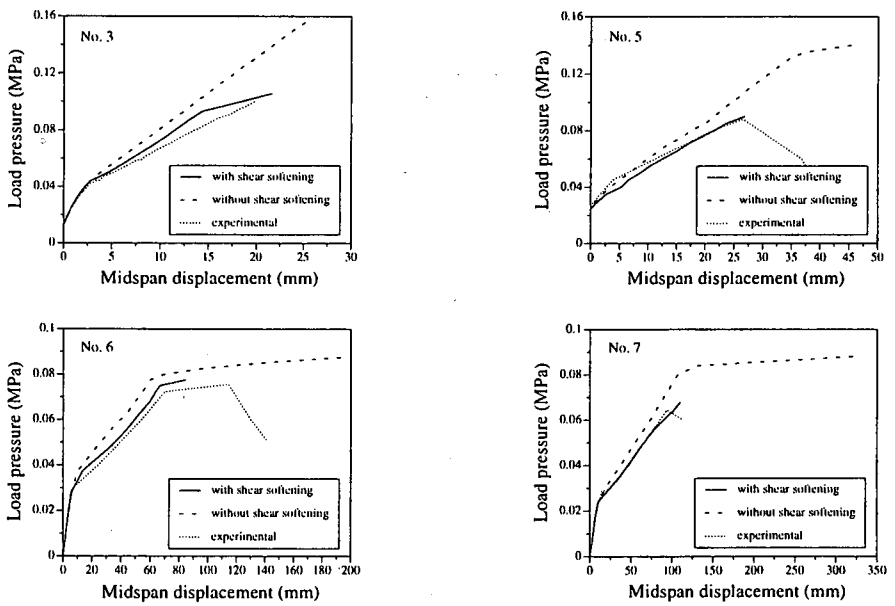

Fig. 26 Numerical results without shear softening model

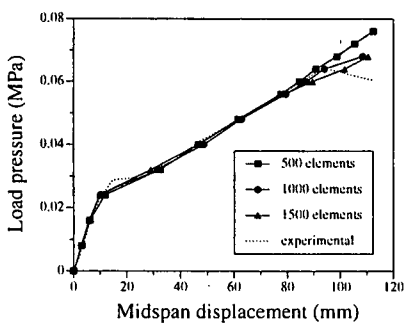

Fig. 27 Load pressure-midspan displacement curves for different mesh

displacement responses are shown in **Fig. 27**. Although the analysis results exhibit small scatter for the loading capacity, the predictions are close to the experimental results. The mesh sensitivity has been reduced, yet the loading capacity when the specimen has 500 elements is higher than that of the other specimens. The finer mesh is recommended since the larger element size will restrict potential crack direction.

5. CONCLUSIONS

This paper has presented a practical, computationally efficient procedure for simulating fracture of reinforced concrete structures. Special attention was paid to the new approaches for modeling the actions of reinforcing steel in concrete material. The Kawai's spring network model with random geometry is used as a basis to represent the concrete material. Reinforcing material is explicitly modeled

using a regular beam and special linkage element. Reinforced concrete piers and beams were analyzed to confirm applicability and effectiveness of the proposed spring network model. The following conclusions are led through this research:

1) The simplicity of the concrete model provides a natural means for incorporating discrete models of reinforcing material. Reinforcement, which consists of a series of beam elements, is introduced explicitly, so that the bonding action between the reinforcement and the matrix material can be modeled with special linkage elements.

2) Mesh construction in this approach is greatly facilitated. The matrix material is discretized semi-automatically with random geometry, which reduces a mesh bias on crack development. Reinforcing steel can be positioned without regard to the concrete mesh design. Since model-preprocessing efforts are greatly reduced, the approach can be applied as a practical means for integrating analyses and design process in reinforced concrete structures.

3) The analyses of reinforced concrete structures give the reasonable results in load-displacement responses, historical curves of strain in reinforcing steel, and especially crack patterns. Crack initiation and propagation of concrete are presented realistically. The model predicts not only flexural failure but also shear failure of reinforced concrete. Discrete modeling of concrete and reinforcing material can be used for understanding of fracture behavior in reinforced concrete structures.

ACKNOWLEDGEMENT: The kind support provided by the Japan Society for the Promotion of Science for Young Scientists to the first author is gratefully acknowledged.

REFERENCES

1) Ngo, D. and Scordelis, A. C. : Finite element analysis of reinforced concrete beams. *American Concrete Institute Journal*, Vol. 64, pp.152-163, 1967.
2) Kawai, T. : New discrete models and their application to seismic response analysis of structure. *Nuclear Engineering and Design*, Vol. 48, pp. 207-229, 1978.
3) Toi, Y. and Che, J. S. : Mesoscopic simulation of microcracking behaviors of brittle polycrystalline solids. *Proceedings of the Japanese Society of Mechanical Engineers*, Vol. 59, pp. 240-247, 1993. (in Japanese)
4) Liu, Y.-Q., Hikosaka, H. and Bolander, J. E. : Modeling compressive failure using rigid particle systems. *Fracture Mechanics of Concrete Structures*, ed. Wittmann F. H., Aedificatio Publishers, Freiburg, Germany, pp. 375-382, 1995.
5) Ueda, M., Takeuchi, N., Higuchi, H. and Kawai, T. : A discrete limit analysis of reinforced concrete structures. *Computer-Aided Analysis and Design of Concrete Structures*, eds. Damjanic, F., Hinton, E., Owen, D. R. J., Bicanic, N. and Simovic, V., Pineridge Press, Swansea, United Kingdom of Great Britain, pp. 1369-1384, 1984.
6) Jagota, A. and Bennison, S. J. : Spring-network and finite element models for elasticity and fracture. *Nonlinearity and Breakdown in Soft Condensed Matter*, eds. Bardhan, K. K., Chakrabarti, B. K. and Hansen, A., Springer, Berlin, 1994.
7) Schlangen, E. and Garboczi, E. J. : New method for simulating fracture using an elastically uniform random geometry lattice, *International Journal of Engineering Science*, Vol.34, pp. 1131-1144, 1996.
8) Bolander, J. E. and Saito, S. : Fracture analyses using spring network models with random geometry. *Engineering Fracture Mechanics*, Vol. 61, pp. 569-591, 1998.
9) Bazant, Z. P. : Microplane model for strain-controlled inelastic behaviour, *Mechanics of Engineering Materials*, eds. Desai, C. S. and Gallagher, R. H., John Wiley & Sons Ltd, London, pp. 45-59, 1984.
10) Ueda, M., Kambayashi, A., Kito, H. and Takeuchi, N. : Size effect analysis using RBSM with Voronoi elements, *Size Effect in Concrete Structures*, eds. Mihashi, H., Okamura, H. and Bazant, Z. P., E & FN Spon, London, pp. 221-232, 1994.
11) Preparata, F. P. and Shamos, M. I. : *Computational Geometry – An Introduction*. Springer-Verlag Inc., New York, 1985.
12) Owen, D. R. J., Figueiras, J. A. and Damjanic, F. : Finite element analysis of reinforced and prestressed concrete structures including thermal loading, *Computer Methods in Applied Mechanics and Engineering*, Elsevier Science Publishers, North-Holland, Vol. 41, pp.323-366, 1983.
13) Nakamura, S., Kitsutaka, Y., Mihashi, H. and Uchida, Y. : Discussion on standard evaluation method for tension softening properties of concrete, *Concrete Research and Technology*, JCI, Vol. 10, pp.151-164, 1999. (in Japanese)
14) Bolander, J. E. and Hikosaka, H. : Characterizing the fracture process in concrete using nonlocal continuum FE modeling, *Theoretical and Applied Mechanics*, University of Tokyo Press, Vol. 40, pp.319-326, 1991.
15) Ueda, M., Takeuchi, N., Higuchi, H., Kito, H. and Kawai, T. : Discrete limit analysis of reinforced concrete structures including the effects of tensile and compressive failure, *Journal of Structural Engineering*, JSCE, Vol. 36A, pp.315-323, 1990. (in Japanese)
16) Van Mier, J. G. M. : *Fracture Processes of Concrete*. CRC Press Inc., New York, 1997.
17) Aoyagi, Y. and Yamada K. : Strength and deformation characteristics of reinforced concrete shell elements subjected to in-plane forces. *Proceedings of Japan Society of Civil Engineers*, Vol. 331, pp. 167-180, 1983. (in Japanese)
18) Saito, S. and Bolander, J. E. : Numerical analyses of shrinkage cracking controlled by carbon fiber nets. *Proceedings of the Third International Symposium on Non-Metallic (FRP) Reinforcement for Concrete Structures*, Sapporo, Japan, Vol. 2, pp. 275-282, 1997.

19) Comité Euro-International du Béton : *CEB-FIP Model Code 1990 First Draft*. CEB, Paris, 1990.
20) Hikosaka, H., Satake, M., Matsushita, H. and Bolander, J. E. : Reinforcing details in concrete T-shape piers under eccentric loadings. *Journal of Structural Engineering*, JSCE, Vol. 38, pp. 1245-1254, 1992. (in Japanese)
21) Hsu, T. T. C. : *Unified Theory of Reinforced Concrete*, CRC press Inc., Boca Raton, 1993.
22) Iguro, M., Shioya, T., Nojiri, Y. and Akiyama, H. : Experimental studies on the shear strength of large reinforced concrete beams under uniformly distributed load. *Proceedings of Japan Society of Civil Engineers*, Vol. 348, pp. 175-184, 1984. (in Japanese)
23) Shirai, N. : JCI round robin analysis of size effect in concrete structures. *Size Effect in Concrete Structures*, eds. Mihashi, H., Okamura, H. and Bazant, Z. P., E & FN Spon, London, pp. 295-322, 1994.
24) An, X., Maekawa, K. and Okamura, H. : Numerical simulation of size effect in shear strength of RC beams. *Journal of Materials, Concrete Structures, and Pavements*, JSCE, Vol. 564, pp. 297-316, 1997.

(Received October 6, 1998)

バネ系モデルを用いた鉄筋コンクリート構造物の破壊挙動の数値解析

斉藤成彦・彦坂　熙

コンピューターを用いた数値解析法は，コンクリートの破壊メカニズムを包括的に理解する上で最も有効な手段の一つである．本研究では，鉄筋コンクリート構造物を解析するための実践的で効果的な数値解析モデルを提案する．コンクリートは，ランダムな形状の要素分割を用いた剛体ーバネモデルによりモデル化する．剛体ーバネモデルでは，鉄筋の特性をコンクリート要素内に一様に分散させるモデルが一般的であるが，本研究では鉄筋を離散的に扱うモデルを提案する．本モデルは，コンクリートのひびわれをより実際に近い形で表現できる．鉄筋コンクリート張り出し式橋脚と大型鉄筋コンクリートはりの破壊挙動の数値解析例を示し，実験結果と比較検討を行った．